Proceedings of Meetings on Acoustics

Volume 19, 2013 http://acousticalsociety.org/


**ICA 2013 Montreal**
**Montreal, Canada**
**2 - 7 June 2013**

**Architectural Acoustics**
**Session 4pAAa: Room Acoustics Computer Simulation II**

# 4pAAa2. Modeling (Non-)uniform scattering distributions in geometrical acoustics

**Dirk Schröder* and Alexander Pohl**

***Corresponding author's address: EPFL, Lausanne, 1015, Vaud, Switzerland, dirk.schroeder@epfl.ch**

In most cases, a surface is not ideally smooth. It rather contains regular and irregular dents, bumps and other textures that influence the reflection of the incident wave. A reflection on such a corrugated surface causes a frequency-dependent redirection of the incident sound energy outside the specular direction, called scattering. While the computation of the specular part is well elaborated today, a model that thoroughly captures the wave phenomenon of scattering is still under discussion. Here, the most common assumption is that scattered energy follows a uniform Lambert distribution, which has proven to be a good approximation, especially in room acoustical applications. In this contribution, we will discuss Lambert-based scattering models (specular/diffuse sound field decomposition and vector mixing) and their implementations in methods of Geometrical Acoustics. We will analyze benefits and flaws of the respective models and investigate possibilities to introduce angle-dependent scattering for use cases where the uniform Lambertian distribution becomes invalid.

Published by the Acoustical Society of America through the American Institute of Physics

 [DOI: 10.1121/1.4800288]
Received 22 Jan 2013; published 2 Jun 2013

## INTRODUCTION

If a plane wave hits an infinitely large and smooth medium, it will be reflected on the surface according to Snell's law (the angle of incidence is equal to the angle of reflection), whereby a certain fraction of the sound wave's energy is absorbed. In practical cases, however, surfaces have irregular textures and are of finite size, which both cause – in addition to the specular reflection – a scattering of the sound wave[1], i.e., a distinct portion of the reflected sound wave energy is scattered into non-specular directions. The wave effect of scattering is strongly frequency-dependent and mainly occurs if the height and length of the surface's corrugation profile are in the order of half of the wavelength $\lambda$. In contrast, if the wavelength is very large in comparison to the surface's irregularities, the surface will appear smooth for the striking wave front, whereas the wave will be specularly reflected on the texture's faces and not on the surface's plane if the wavelength is very small. In other words, a reflection on a corrugation surface can be understood as a decomposition of the wave front into a specularly reflected and a diffusely reflected sound energy portion.

Especially in the room acoustics design of performance facilities such as concert halls, diffuse reflecting surfaces play an important role since they help to reduce (flutter-) echoes and noise, and create a more homogenous temporal and spatial density of the reverberant sound [1]. But even in more ordinary rooms with rather smooth surfaces such as offices or classrooms, a dominance of scattered energy in the reverberation process can be observed [2]. Therefore, it is common sense to include some type of scattering implementation in room acoustics prediction tools based on Geometrical Acoustics (GA) in order to produce more accurate predictions [3, 4].

Today, most scattering implementations rely on Lambert's cosine law, which actually originates from optics, but has proven in the past to be a good approximation for many everyday use cases. However, implementations vary in the modeling of the directional distribution of diffuse reflections [5]. Inspired by Dahlenbäck's presentation at Forum Acusticum 2011 [6] in Aalborg, Denmark, we decided to further investigate the two most-commonly applied scattering implementations, namely the Hybrid Reflectance Model (HRM) and Vector Mixing (VM). By analytically deriving and subsequently analyzing probability density functions of possible reflection angles, we hope to give further insights on the directional behavior of both methods. To make this more transparent, we restrict all investigations to 2D.

## SCATTERING MODELS

In the following, the HRM and VM shall be briefly described. Both models utilize the ubiquitous Lambert function and rely on traditional Sound Particle Simulation Method (SPSM), which – in short – emulates the propagation of a sound impulse from a sound source by means of energy particles. These particles travel on discrete rays, become reflected on geometric objects, and are detected by (volume) receivers in order to compute the respective energy envelope of the Room Impulse Response (RIR). A SPSM simulation starts by emitting a finite number of particles that are evenly distributed on the source's surface and travel with the speed of sound. Each particle carries a certain amount of energy that usually depends on the source's directional pattern. While propagating, each particle loses energy due to air absorption and occurring reflections, i.e., surface-dependent absorption and scattering of sound. Each particle is traced until a predefined termination condition is fulfilled, e.g., exceeded simulation length or under-run of a minimum particle's energy threshold.

**Hybrid Reflectance Model** The HRM strictly decomposes a sound reflection into both a specularly reflected and a diffusely reflected sound energy portion, $E_{r,specular}$ and $E_{r,diffuse}$,

$$E_{r,specular} = (1-s)\cdot E_r, \quad E_{r,diffuse} = (s)\cdot E_r, \quad with \quad E_r = (1-\alpha)\cdot E_i, \tag{1}$$

[1]The two main mechanisms of wave scattering are surface roughness and edge diffraction.

where $E_i$ is the incident energy, $E_r$ describes the total reflected energy, $\alpha$ the absorption coefficient and $s$ the scattering coefficient of the hit surface. The scattered energy is assumed to be distributed according to Lambert's cosine law, i.e., the intensity of a reflected particle is independent of the angle of incidence but proportional to the cosine of the angle of reflection. The strict separation of sound energy additionally enables an individual processing of both types of reflections, such as using the Image Source Method (ISM) for the specular part and SPSM for the diffuse part, e.g., [1, 2, 7]. However, we will focus on pure stochastic SPSM in the following since it makes the model explanation better comparable to VM.

In a traditional SPSM implementation, the decision whether a reflection is specular or diffuse is made by comparing a random number between {0,1} with the assigned scattering coefficient $s$ of the surface that was hit by an energy particle (the standardized scattering coefficient is defined as the ratio between the non-specularly reflected energy to the totally reflected energy [8]). If the random number is greater than $s$, a specular reflection will occur, otherwise, the particle gets reflected in random direction following a Lambertian distribution of the reflection angle (see Fig. 1a, the respective direction vector $\vec{v}_{out}$ of the reflection is given either by the unit vectors $\vec{e}_{spec}$ or $\vec{e}_{scat}$, depending on the current reflection type). It should be noted that the particle's energy weighting with $s$ (diffuse reflection) or $(1-s)$ (specular reflection), as described in Equ. 1, is already included in such a pure stochastic implementation due to the reflection type decision by random numbers.

**Vector Mixing** In contrast to the HRM, VM, e.g., [9, 10], directly combines specular and diffuse reflections instead of handling them separately. The idea is to calculate the particle's direction of reflection $\vec{v}_{out}$ by a vector addition of the specular unit vector $\vec{e}_{spec}$, scaled by $(1-s)$, and the diffuse unit vector $\vec{e}_{scat}$, scaled by $s$, and following a certain direction distribution, with

$$\vec{v}_{out} = (1-s)\cdot\vec{e}_{spec} + s\cdot\vec{e}_{scat}. \tag{2}$$

Today, at least four types of VM exist [6], which all follow the same principle as described above, but differ in the direction distribution of the diffuse unit vector $\vec{e}_{scat}$. In this contribution we choose the most straightforward VM model as illustrated in Fig. 1b, where the determination of $\vec{e}_{scat}$ is identical to HRM. In addition, this VM model yields the same results as the HRM for the two cases a) 'only specular reflections' ($s = 0$) and b) 'only diffuse reflections' ($s = 1$), as one can directly see from Equ. 2 and Fig. 1b. However, the two models differ extremely in between these two extrema of the scattering coefficient, which will be thoroughly discussed in the next section by analyzing analytical probability density functions of the reflection angle.

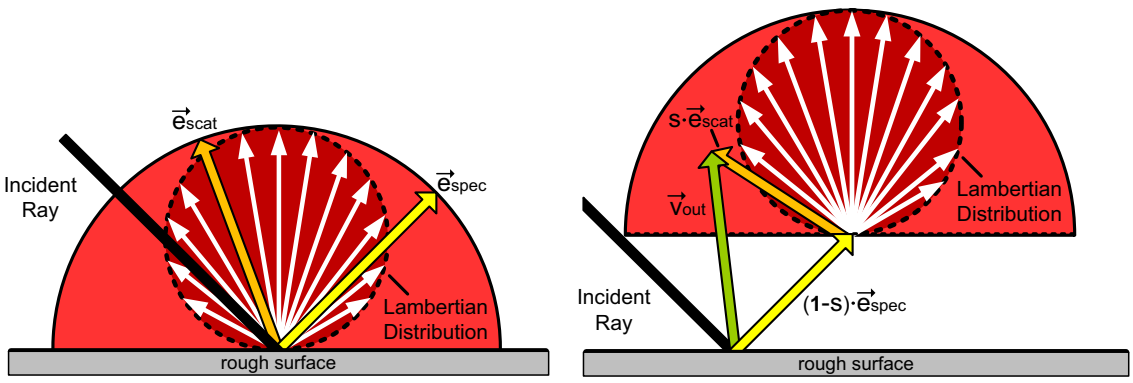


**(A) Hybrid Reflectance Model**. Specular and diffuse reflections are handled separately from each other, denoted by the unit vectors $\vec{e}_{spec}$ and $\vec{e}_{scat}$.

**(B) Vector Mixing**. The resulting direction of reflection is computed by a vector combination of the weighted unit vectors $(1-s)\cdot\vec{e}_{spec}$ and $s\cdot\vec{e}_{scat}$.

**FIGURE 1:** Schematic drawings of the two analyzed scattering models.

## Reflection Angle Probability Density Function

In order to compare the two presented scattering models in a proper way, we analytically derive Reflection Angle Probability Density Functions (RAPDFs) for both methods first. A RAPDF describes angle-wise the probability for a striking energy particle to get reflected under a certain angle $\vartheta_{out}$ for a given incidence angle and a given scattering coefficient. A normalization is applied to the RAPDFs such that the integral over the RAPDF's complete angle range equals one.

**Hybrid Reflectance Model** In case of the HRM, two RAPDFs exists due to the strict separation of specular and diffuse reflections, denoted as $RAPDF_{HRM,spec}$ and $RAPDF_{HRM,scat}$ in the following. The determination of the RAPDFs is in both cases obvious and their computation straightforward. While for the specular reflection the $RAPDF_{HRM,spec}$ is just a Dirac Delta function at $\vartheta_{out}$=$\vartheta_{spec}$, i.e., the specular angle of reflection, $RAPDF_{HRM,scat}$ is identical with the Lambertian distribution, i.e., $\vartheta_{out} = \vartheta_{Lambert}$. Both functions are scaled by $(1-s)$ and $s$, respectively, which relates to the probability of the occurrence of each reflection type since this decision is made by drawing random numbers (see previous section). Thus, the RAPDFs conclude to

$$RAPDF_{HRM,spec} = (1-s)\cdot\delta(\vartheta_{out}-\vartheta_{spec}) \quad and \quad RAPDF_{HRM,scat} = s\cdot\frac{cos(\vartheta_{Lambert})}{2}, \qquad (3)$$

where an example is illustrated in Fig. 2a for an angle of incidence of $\vartheta_{in}$ =45° and different values of the scattering coefficients $s$.

**Vector Mixing** In contrast to the previous case, the analytical derivation of the RAPDF for VM is quite demanding from a mathematical point of view and has to be done in several steps that can only be outlined due to space restrictions. However, the complete derivation can be downloaded at `www.openMeasurements.net` as MATLAB® script that features also a handy and intuitive graphical user interface. We encourage the interested reader to download this script since it gives valuable insights on the behavior of both scattering models that cannot be summarized in only one paper.

As described in the previous section, the particle's direction of reflection $\vec{v}_{out}$ is computed by the vector combination of the scaled unit vectors $\vec{e}_{spec}$ and $\vec{e}_{scat}$ (compare Equ.2), which can also be written as a function of the (fixed) specular angle of reflection $\vartheta_{spec}$ and the Lambertian

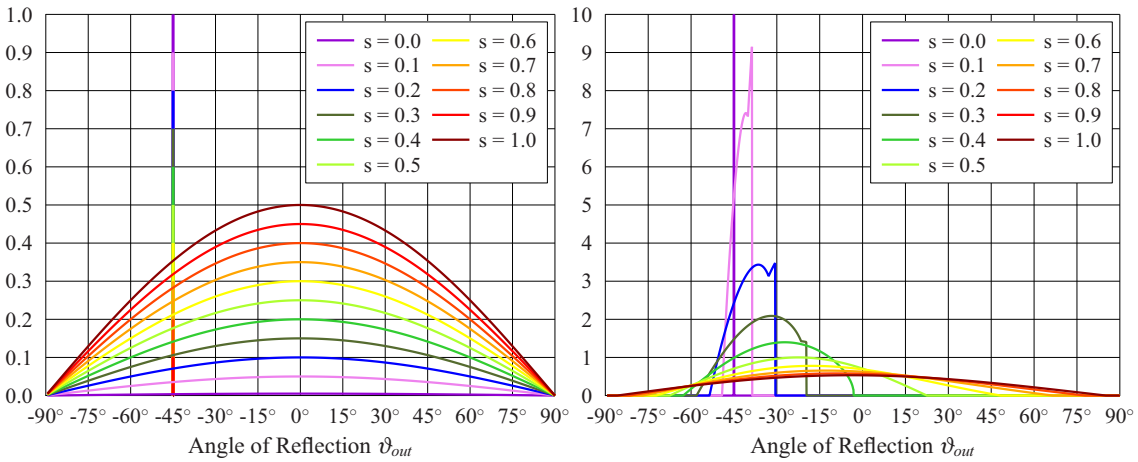


**(A) Hybrid Reflectance Model.** **(B) Vector Mixing.**

**FIGURE 2:** Analytically derived RAPDFs of the HRM and VM for a fixed angle of incidence of $\vartheta_{in}$ =45°, but varying scattering coefficients. The direction of the surface normal relates to 0°.

distributed angle $\vartheta_{Lambert}$, with

$$\vec{v}_{out} = \begin{pmatrix} (s-1)\cdot sin(\vartheta_{spec}) & - & s\cdot sin(\vartheta_{Lambert}) \\ (1-s)\cdot cos(\vartheta_{spec}) & + & s\cdot cos(\vartheta_{Lambert}) \end{pmatrix}. \quad (4)$$

From this expression, we can directly derive the particle's angle of reflection $\vartheta_{out}$ as a function of $\vartheta_{Lambert}$ using the atan2 function, with $\vartheta_{out} = f(\vartheta_{Lambert}) = -atan2(\vec{v}_{out,x}, \vec{v}_{out,y})$. In order to determine the RAPDF, however, we have to invert this function since we actually need an expression for $\vartheta_{Lambert}$ as a function of $\vartheta_{out}$, i.e., $\vartheta_{Lambert} = g(\vartheta_{out})$. Once this inverse function is found, the last step is to insert $g(\vartheta_{out})$ into the Lambertian probability density function and an analytical expression for the RAPDF is found, with $RAPDF_{VM} = p(\vartheta_{Lambert}) = p(g(\vartheta_{out}))$.

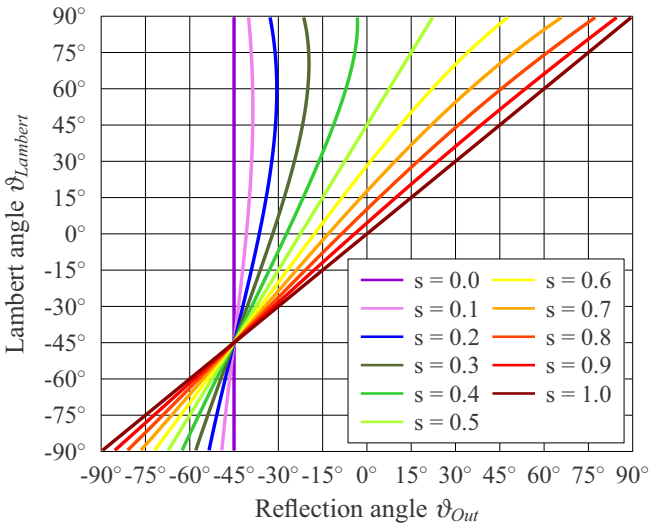


**FIGURE 3:** $\vartheta_{Lambert} = f(\vartheta_{Out})$ and $\vartheta_{In} = 45°$

Unfortunately, the inversion of $f(\vartheta_{Lambert})$ turns out to be quite complex. Problems mainly occur for small scattering coefficients $s$, where multiple Lambert angles $\vartheta_{Lambert}$ result in the same reflecting angle $\vartheta_{out}$ (compare Fig. 3). This ambiguity turns the function into a relation and the sought-after inversion can only be determined as a complicated piecewise solution. An example of the $RAPDF_{VM}$ is depicted in Fig. 2b for the identical case as for the HRM (angle of incidence of $\vartheta_{in}$ =45° and different values of $s$). Most noticeable are the occurring spikes in the case of rather specular reflections (low values of $s$). These disruptions come from geometrical issues during the construction of $\vec{v}_{out}$, which is further illustrated in Fig. 4. For rather high values of $s$, $\vartheta_{out}$ will always lie within the lime green-colored area (see Fig. 4a). Therefore, the upper and lower boundary of $\vartheta_{out}$ coincidence with the minima of the Lambert distribution ($\vartheta_{Lambert} = \pm 90°$) resulting in smooth RAPDFs (see Fig. 2b, $s \geq 0.5$). Unfortunately, this does not hold for lower values of $s$ as one can directly see in Fig. 4b. In this case, one of the boundaries of $\vartheta_{out}$ is shifted to the tangent line to the semi circle (red area) resulting in an extension of the possible angle range of $\vartheta_{out}$ (dark green-colored area in Fig. 4b). This circumstance exactly causes the observed spikes due to the Lambertian distribution of $\vec{e}_{scat}$.

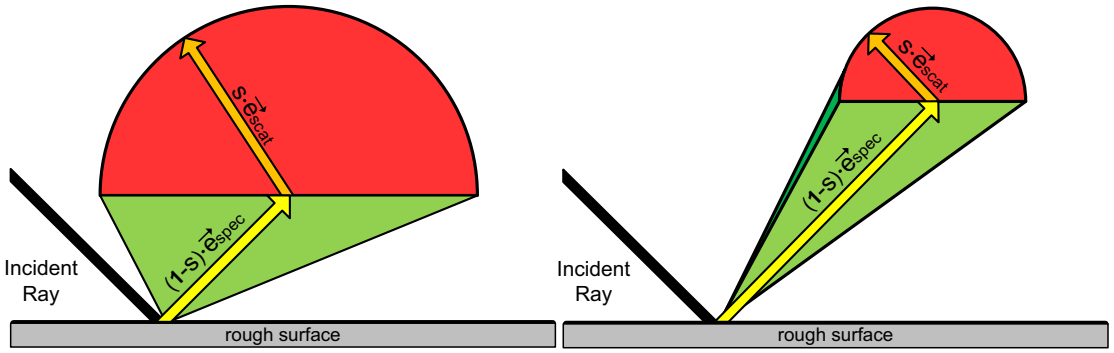


**(A)** Reflections rather diffuse (high values of $s$). **(B)** Reflections rather specular (low values of $s$).

**FIGURE 4:** Boundaries of the reflection angle $\vartheta_{out}$, denoted as lime green and dark green colored areas.

From this it follows, that the probability distribution of $\vartheta_{out}$ starts with a value unequal to zero, decreases according to Lambert until the lime-green area is reached, and increases again. It is questionable if this behavior is in compliance with real-world processes.

## Comparison of Scattering Models

Both scattering models are hardly comparable by analyzing only their RAPDFs. For practical cases, it is more important to evaluate their impact on the simulation results. Therefore, both scattering models are applied to a 2D-SPSM in order to compare them for simple test cases.

### Single Surface

**Simulation Setup** To compute the sound intensity for a given source/receiver position, a 2D-SPSM simulation with $N = 2000$ primary sound particles is carried out (see Fig. 5a). Each surface-striking primary sound particle is split up into $S = 200$ secondary sound particles, where the energy of each secondary sound particle is computed by integrating the RAPDF over the respective angle range (see Fig. 5a, purple region). The detection of the direct sound (directly impacting primary sound particles on the receiver surface) is always skipped since we want to focus on first-order reflections only. In order to achieve results that are independent of the source power, a transmission degree $T$ is introduced (similar to [11]) that normalizes the computed sound intensity to a reference sound intensity given by the equivalent image source.

In the following, all distances are dimensionless since only the aspect ratio is of interested. Angles are always given in relation to the surface's reference point $P$ and the surface normal, i.e., the normal itself corresponds to 0°. The sound source is located at $\varphi_S = 45°$ with a distance of $r_S = 20$ to the reference point $P$. Fifteen receivers are positioned on a semi circle having a radius of 10 and with $P$ as center. The receivers are distributed in increments of 12°, i.e., in the range of $-84 <° \varphi_R < +84°$. The detector size is chosen such that neighboring receivers are always tangent to each other. The whole setup is depicted in Fig. 5b.

**Infinite Surface** The most simplest case is an infinite 1D-surface with constant scattering coefficient $s$ and no absorption $\alpha = 0.0$. The respective computed transmission degrees for this setup are given in Fig. 6. As expected, both scattering models behave almost identically for the two extreme cases of 1) 'only specular' ($s = 0.0$) and 2) 'only diffuse' ($s = 1.0$) reflections. In the first case ($s = 0$), a pure specular reflection has to be modeled by both methods expecting a

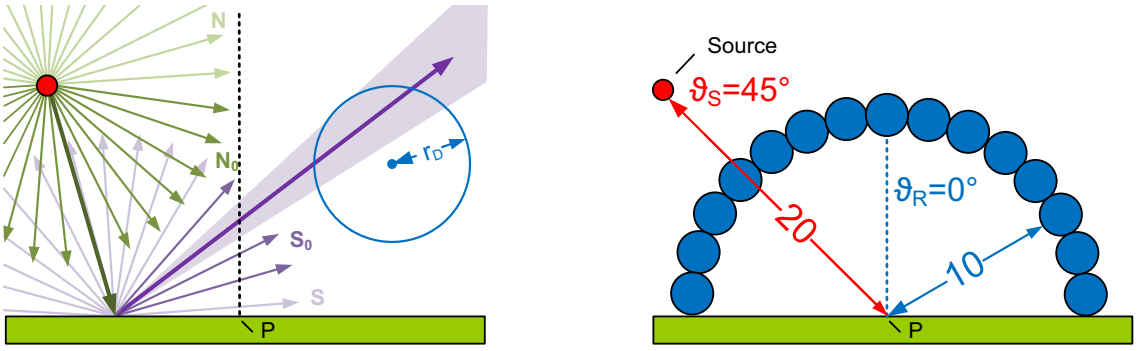


**(A)** Recursive split-up of sound particles by a scattering surface

**(B)** Source and receiver positions above a scattering surface.

**Figure 5:** Definitions for a single scattering surface.

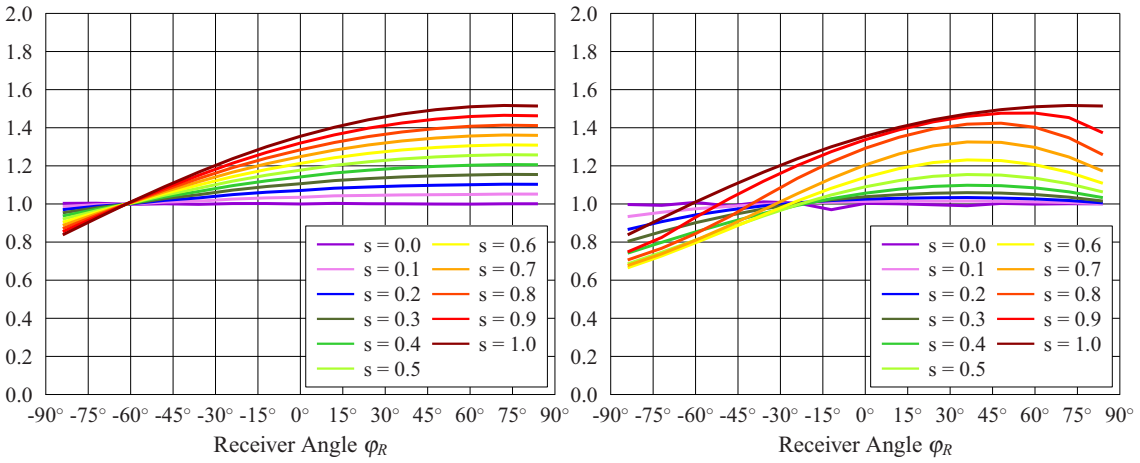


**(A) Hybrid Reflectance Model.** **(B) Vector Mixing.**

**FIGURE 6:** Transmission degree $T$ for an infinite surface. The sound source is fixed at $\varphi_S = +45°$, $r_S = 20$ and 15 receivers are evenly distributed on a semi circle having a radius of $r_R = 10$.

transmission degree of $T = 1$ since the detected sound intensity is equal to the sound intensity given by the corresponding image source. While HRM flawlessly handles this specular reflection by means of the dedicated Dirac delta pulse (see previous section), it can only be approximated by VM resulting in some minor numerical problems. In the second case ($s = 1.0$), a maximum transmission degree of $T \approx 1.4$ is observed for $\varphi_R = +84°$, whereas a minimum transmission degree of $T \approx 0.8$ is reached for $\varphi_R = -84°$ (identical for both models). In between these two extrema, the scattering models behave quite differently. While a linear transition is observable for the HRM, VM shows a maximum transmission degree at $\varphi_R = 45°$ for $0.1 < s < 0.9$.

### Finite Surface

In a second experiment, the 1D-surface is limited to an overall length of $2 \cdot a_{Max}$ with the reference point $P$ lying halfway between both ends. This time, the surface has still the same absorption factor of $\alpha = 0.0$ as in the infinite case, but a fixed scattering coefficient of $s = 0.5$. The

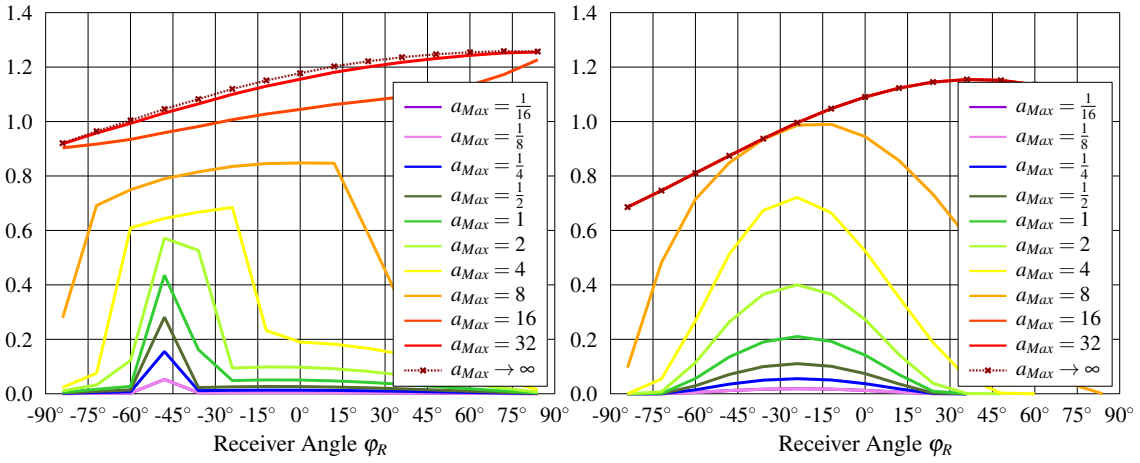


**(A) Hybrid Reflectance Model.** **(B) Vector Mixing.**

**FIGURE 7:** Transmission degree $T$ for a finite surface of length $2 \cdot a_{Max}$. The sound source is fixed at $\varphi_S = +45°$, $r_S = 20$ and 15 receivers are evenly distributed on a semi circle having a radius of $r_R = 10$. The scattering coefficient is set to $s = 0.5$.

corresponding transmission degrees for $\frac{1}{16} < a_{Max} < 32$ are shown in Fig. 7 ($a_{Max}$ is always increased by a factor 2).

With increasing surface size, the behavior of both methods converges to the respective transmission degrees of the infinite surface (compare with Fig. 6, $s = 0.5$) and only slight differences occur for surfaces $a_{Max} \geq 32$ (in case of VM even for $a_{Max} \geq 16$). For smaller distances, smaller transmission degrees can be noticed for both methods, but the overall transmission degree is more smoothly distributed for the VM than for the HRM. In addition, the maximum of the HRM is exactly at the angle of specular reflection $\varphi_R = -45°$, whereas it is translated to $\varphi_R \approx -30°$ in the case of the VM. For very small surfaces, only one receiver remains that detects energy at $\varphi_R = -45°$ (HRM), whereas even for the smallest surfaces multiple receivers detect energy with VM. Physically speaking, the HRM keeps the specular part of the reflection even for small surfaces, whereas the VM automatically smears the reflected energy among a larger angle range.

## Rectangular Room

To complement the investigations with a more practical use case, simulations are carried out for a rectangular 2D-room ($L = 10m$ and $H = 5m$, i.e., with a proportion factor of q= H/L=0.5) in order to analyze the impact of both models on the Reverberation Time (RT). While the two larger extended (1D-) surfaces $L$ are completely absorbent ($\alpha = 0.0$, $s = 0.0$), the scattering coefficient of the smaller surfaces $H$ is varied ($\alpha = 0.0$, $0 \leq s \leq 1.0$). As this setup results in a strong flutter echo[12], the only reduction of sound energy propagating in between the reflecting surfaces $H$ is caused by scattering, since all scattered energy is absorbed that travels in direction to the larger surfaces $L$. From this it follows that the computed RT is a measure of the overall scattering strength, because more scattered sound energy ends up with smaller RTs.

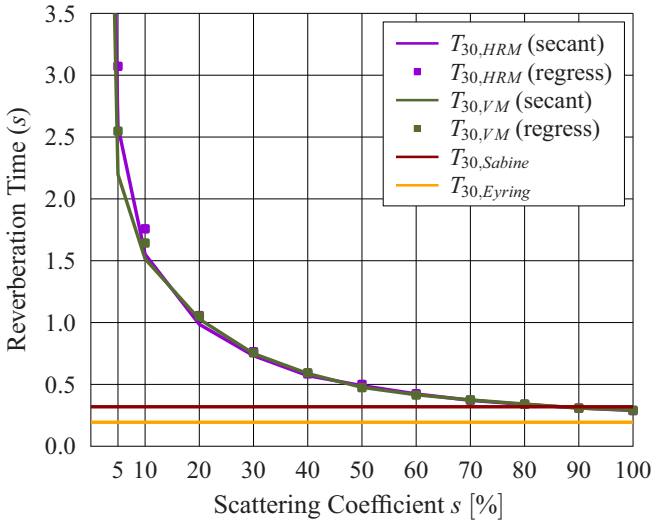


**FIGURE 8:** Reverberation time ($T_{30}$) computed for a rectangular room utilizing the HRM and VM.

To achieve significant results, $N = 125{,}000$ sound particles are sent out omnidirectional from a sound source located in the center of the room, and traced over a maximum of 200 reflections (empirically corresponding to a relative error of about 1% in the RT). All computed $T_{30}$-values are – similar to common standards – the times for an energy decay down to $-30dB$ of the total emitted energy, evaluated from the moment just after the first reflection and extrapolated to a $-60dB$ decay. Both a value according to the slope of the secant at the decay curve and the slope by linear regression are determined. As expected, the RTs are drastically dependent on the scattering coefficient of the front walls $H$, especially for low values of $s = 0...10\%$ (see Fig. 8). For $s = 0\%$, the RT is about 8 times higher than for $s = 10\%$ , and over 40 times higher than for $s = 100\%$ – which is in compliance with the Sabine value, but not the Eyring value as expected for highly absorbing rooms. Evaluating the decay by regression, the RT at $s = 0\%$ is almost 2 times higher. The influence of the chosen scattering model is (with these high numbers of sound particles) neglectable, except for small values of $s = 5 - 10\%$, where the HRM yields about about 20% higher RTs.

## Conclusion and Outlook

In this contribution, we presented analytical descriptions for the scattering distributions of the two most-commonly applied scattering models HRM and VM. Both methods showed identical results for the extreme cases of $s = 0.0$ and $s = 1.0$ in all experiments. For scattering coefficients in between those extreme values, the VM method yields on average higher effective scattering than the HRM.

The presented analytical formulations have to be extended to full 3D scenarios and complex setups. In addition, the analytical descriptions may be used to determine scattering coefficients by comparing the RAPDFs with measured or computed energy distributions. However, angle-dependent energy distributions are also applicable and should be used to describe special types of geometries that scatter in a preferred direction, e.g., [8, 13].

## References

[1] H. Kuttruff, *Room Acoustics, 4th edition* (Elsevier) (2000).

[2] M. Vorländer, *Auralization – Fundamentals of Acoustics, Modelling, Simulation, Algorithms and Acoustic Virtual Reality* (Spinger-Verlag Berlin) (2007).

[3] M. Vorländer, "International Round Robin on room acoustical computer simulations", in *Proceedings of the 15th International Congress on Acoustics* (Trondheim, Norway) (1995).

[4] I. Bork, "A comparison of room simulation software – the 2nd Round Robin on room acoustical computer simulation", Acta Acustica United with Acustica **86**, 943 (2000).

[5] B.-I. Dalenbäck, M. Kleiner, and U. Svensson, "A Macroscopic View of Diffuse Reflection", Journal of the Audio Engineering Society **42**, 793–807 (1994).

[6] B.-I. Dalenbäck, "Scattering distributions in geometrical acoustics", in *Proceedings of the Forum Acusticum* (Aalborg, Denmark) (2011).

[7] D. Schröder, "Physically Based Real-time Auralization of Interactive Virtual Environments", Ph.D. thesis, RWTH Aachen University (2011).

[8] T. J. Cox, B.-I. L. Dalenbäck, P. D'Antonio, J. J. Embrechts, J. Y. Jeon, E. Mommertz, and M. Vorländer, "A Tutorial on Scattering and Diffusion Coeffcients for Room Acoustic Surfaces", Acta Acustica United with Acustica **92**, 1 (2006).

[9] U. M. Stephenson, "Eine Schallteilchen-Computer-Simulation zur Berechnung der für die Hörsamkeit in Konzertsälen maßgebenden Parameter", Acustica **59**, 1–20 (1985).

[10] C. L. Christensen and J. H. Rindel, "A new scattering method that combines roughness and diffraction effects", in *Proceedings of the Forum Acusticum* (Budapest, Hungary) (2005).

[11] A. Pohl, D. Schröder, U. M. Stephenson, and U. P. Svensson, "Influence of reflecting walls on edge diffraction simulation in geometrical acoustics", in *Proceedings of International Congress on Acoustics* (Montreal, Canada) (2013).

[12] U. M. Stephenson, "Are there simple reverberation time formulae also for partially diffusely reflecting surfaces?", in *Proceedings of Internoise* (New York, America) (2012).

[13] M. Müller-Trapet and M. Vorländer, "In-Situ Measurements of Surface Reflection Properties", in *Proceedings of International Symposium on Room Acoustics* (Toronto, Canada) (2013).